This is an open access article published under a Creative Commons Attribution (CC-BY) License, which permits unrestricted use, distribution and reproduction in any medium, provided the author and source are cited.

CRYSTAL GROWTH & DESIGN

Article

pubs.acs.org/crystal

Proton Transfer, Hydrogen Bonding, and Disorder: Nitrogen Near-Edge X-ray Absorption Fine Structure and X-ray Photoelectron Spectroscopy of Bipyridine−Acid Salts and Co-crystals

Joanna S. Stevens,*[,†] Lauren K. Newton,[†] Cherno Jaye,[∥] Christopher A. Muryn,[§] Daniel A. Fischer,[∥] and Sven L. M. Schroeder*[,†,‡,§]

[†]School of Chemical Engineering and Analytical Science, The University of Manchester, Oxford Road, Manchester M13 9PL, U.K.

[‡]School of Chemical and Process Engineering, University of Leeds, Leeds LS2 9JT, U.K.

[§]School of Chemistry, The University of Manchester, Brunswick Street, Manchester M13 9PL, U.K.

[∥]National Measurement Laboratory, National Institute of Standards and Technology, Gaithersburg, Maryland 20899, United States

Supporting Information

ABSTRACT: The sensitivity of near-edge X-ray absorption fine structure (NEXAFS) spectroscopy to Brønsted donation and the protonation state of nitrogen in the solid state is investigated through a series of multicomponent bipyridine−acid systems alongside X-ray photoelectron spectroscopy (XPS) data. A large shift to high energy occurs for the 1s → 1π^* resonance in the nitrogen K-edge NEXAFS with proton transfer from the acid to the bipyridine base molecule and allows assignment as a salt (C═NH$^+$), with the peak ratio providing the stoichiometry of the types of nitrogen species present. A corresponding binding energy shift for C═NH$^+$ is observed in the nitrogen XPS, clearly identifying protonation and formation of a salt. The similar magnitude shifts observed with both techniques relative to the unprotonated nitrogen of co-crystals (C═N) suggest that the chemical state (initial-state) effects dominate. Results from both techniques reveal the sensitivity to identify proton transfer, hydrogen bond disorder, and even the potential to distinguish variations in hydrogen bond length to nitrogen.

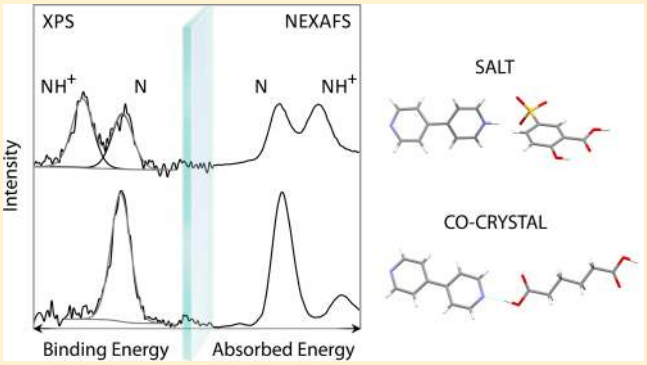

INTRODUCTION

Proton (hydrogen) transfer can be thought of as one of the simplest chemical reactions, ranging from complete transfer from an acidic to a basic moiety (protonation through Brønsted donation) to varying degrees of sharing through hydrogen bonding. Whether Brønsted proton transfer occurs has a profound effect on the location of protons in crystal structures and influences chemical and physical properties. These interactions can be employed to target properties of solid forms (crystal engineering), with particular relevance to the pharmaceutical industry where acid/base guest molecules can be combined with active ingredients to tailor properties such as solubility and bioavailability through formation of salts and co-crystals.[1−4] Other relevant fields are organic ferroelectrics,[5] energetic materials,[6] and the design of materials with targeted optical properties such as color[7] and luminescence.[8,9] Even among hydrogen bonds, the level of interaction with the donor and acceptor atoms can vary significantly, from relatively weak to strong with quasi-covalent character,[10] and there is also the possibility of disordered hydrogen bonds.[11] While X-ray diffraction (XRD) and solid-state nuclear magnetic resonance spectroscopy (ssNMR) are often techniques of choice for structural characterization,[2,11−14] they are not always unambiguous with regard to proton locations (although further clarity can often be obtained by neutron diffraction).[11,13−16] The importance of accurate characterization of salts vs co-crystals based on this relatively small difference in proton location should not be underestimated, particularly with the wider implications for intellectual property and regulatory control in the pharmaceutical industry.[4,17]

X-ray photoelectron spectroscopy (XPS) has recently been shown to unequivocally identify whether intermolecular proton transfer occurs in a range of two-component systems and distinguish protonation (salts) from H-bonding (co-crystals),[14,18−21] as well as the presence of zwitterionic species.[22] This reflects the influence of the local chemical state on the core level binding energy,[19,23−25] resulting in a large positive chemical shift due to proton transfer to nitrogen.[14,18−21] Near-edge X-ray absorption fine structure (NEXAFS) is likewise highly dependent on the local electronic structure, as excitation

Received: December 16, 2014
Revised: February 17, 2015
Published: February 23, 2015

 © 2015 American Chemical Society

DOI: 10.1021/cg5018278
Cryst. Growth Des. 2015, 15, 1776−1783

of core level electrons to bound unoccupied diffuse valence states[26] reveals information related to the local environment and bonding. In particular, the π^* resonances, which reflect the excitation of core level electrons to unoccupied π^* antibonding molecular orbitals (1s $\rightarrow$ π^*) for systems with π character, appear to exhibit chemical sensitivity, distinguishing between different types of functional groups.[27−33] NEXAFS has not, however, been a focus for pharmaceutical solid state studies, being only rarely used[34] and more traditionally associated with absorbed molecules on substrates.[26]

Here we report a study combining XPS and NEXAFS to characterize a series of multicomponent bipyridine−acid systems (Figure 1), exploring the dependency on the chemical

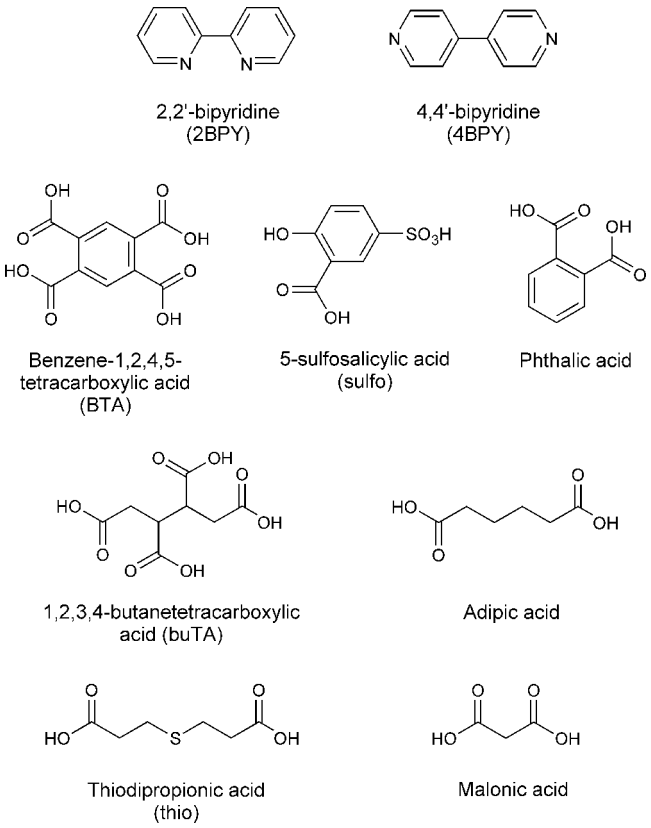

Figure 1. Chemical structures comprising the two component bipyridine−acid (base−acid) systems.

environment of the excited (nitrogen) atom and whether proton transfer has occurred (NH^+ vs N···H−O). Novelty for organic crystal growth research arises from exploiting the sensitivity of NEXAFS π^* resonances to proton transfer. The level of crystallographic information obtainable is explored by looking into the impact of varying nitrogen−hydrogen distance and disorder on NEAXFS and XPS chemical shifts.

EXPERIMENTAL METHODS

Materials. 4,4′-Bipyridine (4BPY), 2,2′-bipyridine (2BPY), 5-sulfosalicylic acid (sulfo) dihydrate, 1,2,3,4-butanetetracarboxylic acid (buTA), and malonic acid were obtained with >99% purity, thiodipropionic acid (thio) with >97% purity, benzene-1,2,4,5-tetracarboxylic acid (BTA) with >96% purity, and phthalic acid and adipic acid with >99.5% purity (Sigma-Aldrich, UK). The salts and co-crystals were formed as follows.

2,2′-Bipyridine/Benzene-1,2,4,5-tetracarboxylic Acid Salt (2BPY/BTA). 2,2′-Bipyridine (156.0 mg, 0.999 mmol) and benzene-1,2,4,5-tetracarboxylic acid (253.6 mg, 0.998 mmol) were each dissolved in 5 mL of ethanol. On combination of the two solutions and stirring, the solution went cloudy and was filtered under vacuum the following day (covered with parafilm with holes overnight) to give the (co-crystal of a) salt $[(2BPY^+)_2{\cdot}BTA^{2-}{\cdot}BTA]$.

4,4′-Bipyridine/5-Sulfosalicylic salt (4BPY/sulfo). 4,4′-Bipyridine (156.8 mg, 1.004 mmol) was dissolved in 4 mL of methanol, and 5-sulfosalicylic acid dihydrate (255.3 mg, 1.004 mmol) was dissolved in 6 mL of methanol. On combination of the two solutions and stirring, a yellow slurry resulted and was filtered under vacuum after 2 h to give the 1:1 salt $[4BPY^+{\cdot}sulfo^-]$.

4,4′-Bipyridine/1,2,3,4-Butanetetracarboxylic Acid Co-crystal (4BPY/buTA). 1,2,3,4-Butanetetracarboxylic acid (352.3 mg, 1.505 mmol) was added to 250 mL of deionized water and heated until the solution was clear. 4,4′-Bipyridine (390.6 mg, 2.501 mmol) was added to 25 mL of water and stirred to give a suspension. The buTA solution was added to the heated 4,4′-bipyridine suspension dropwise over 15 min while stirring. The mixture was left overnight and then filtered to yield the 1:1 co-crystal with some excess starting materials. This initial product was then recrystallized as follows: 123.0 mg of the resulting powder was added to a hot aqueous solution (80 mL, 70 °C) and stirred; additional hot water was added until the product dissolved (total 300 mL). The solution was left to cool to RT, with a small amount of the original product added as a seed the following day. Small, clear crystals started to form after 2 weeks and were filtered after 3 weeks to give the 1:1 co-crystal.

4,4′-Bipyridine/Phthalic Co-crystal (4BPY/phthalic). Stoichiometric amounts of 4,4′-bipyridine (94.4 mg, 0.604 mmol) and phthalic acid (100.3 mg, 0.604 mmol) were milled in a Retsch MM200 mixer mill for 40 min at a rate of 30 Hz, using two 5 mL stainless steel jars, each containing one 7 mm-diameter stainless steel ball, to yield the 1:1 co-crystal.

4,4′-Bipyridine/Adipic Co-crystal (4BPY/adipic). 4,4′-Bipyridine (218.1 mg, 1.396 mmol) was dissolved in 4 mL of methanol, and adipic acid (205.0 mg, 1.403 mmol) was dissolved in 6 mL of methanol. On combination of the two solutions and stirring, the solution went cloudy and was filtered under vacuum after 2.5 h to give the 1:1 co-crystal.

4,4′-Bipyridine/Thiodipropionic Co-crystal (4BPY/thio). 4,4′-Bipyridine (187.1 mg, 1.198 mmol) was dissolved in 5 mL of methanol, and thiodipropionic acid (213.2 mg, 1.194 mmol) was dissolved in 7 mL of methanol. On combination of the two solutions and stirring, the solution went cloudy and was filtered under vacuum after 4 h to give the 1:1 co-crystal.

4,4′-Bipyridine/Malonic Co-crystal (4BPY/malonic). 4,4′-Bipyridine (250.3 mg, 1.603 mmol) was dissolved in 4.5 mL of methanol, and malonic acid (166.6 mg, 1.601 mmol) was dissolved in 5.5 mL of methanol. On combination of the two solutions, the solution went cloudy and was filtered under vacuum after 3 h to give the 1:1 co-crystal.

Successful formation of co-crystals and salts was confirmed by XPS and comparison of X-ray powder diffraction patterns (available as Supporting Information) with those simulated from previously reported single crystal structures.[35−37] The new 4BPY/sulfo system was revealed as a 1:1 salt and 4BPY/buTA system as a 1:1 co-crystal initially by XPS, and this was confirmed by both NEXAFS and single crystal X-ray diffraction (CCDC 1038154 and 1038155, Supporting Information).

Powder X-ray Diffraction (PXRD). Powder X-ray diffraction (PXRD) patterns (available as Supporting Information) were collected using a Rigaku Miniflex instrument utilizing Cu Kα radiation (λ = 1.5406 Å), operating over 5−40° 2θ at 1.5° min^{-1} with a 0.03° step, 30 kV voltage, and 15 mA current. Typically 5 mg of sample was placed on a small sample attachment and smoothed to achieve a level surface.

Single Crystal X-ray Diffraction (XRD). Single crystal X-ray diffraction (XRD) data was collected for 4BPY/sulfo and 4BPY/buTA at 100 K with an Oxford Diffraction X-Calibur 2 diffractometer utilizing Mo Kα radiation (λ = 0.71073 Å) and an Oxford CryoSystems Cryostream Controller 700. Data was recorded at 50 kV and 40 mA with a CCD detector. Data reduction, cell refinement,

DOI: 10.1021/cg5018278
Cryst. Growth Des. 2015, 15, 1776−1783

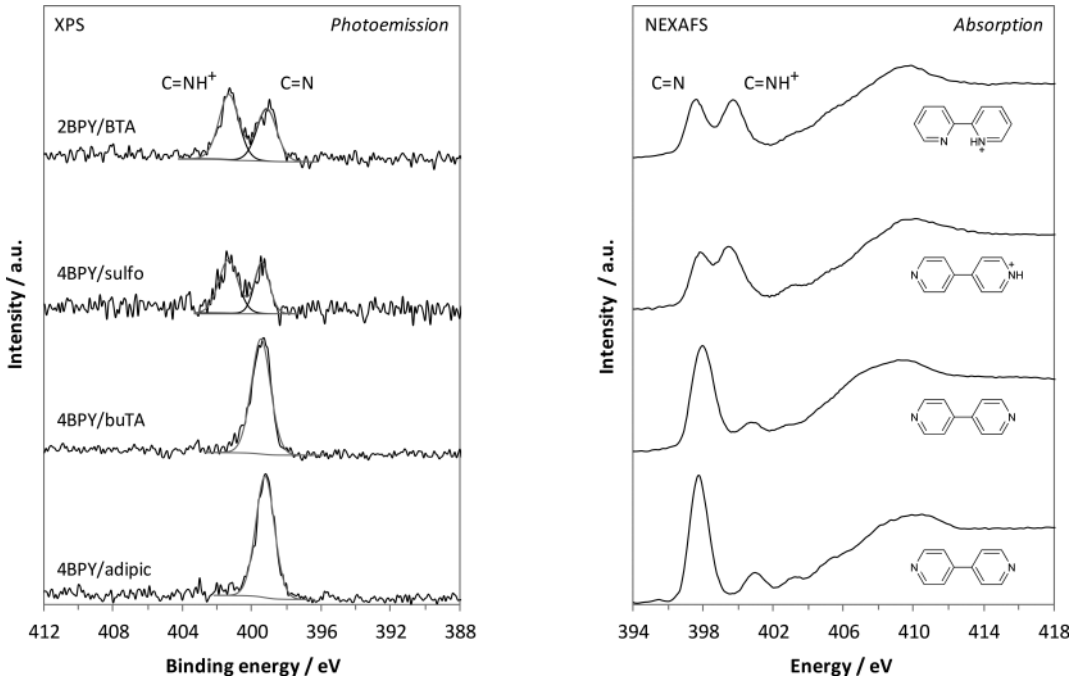

Figure 2. Nitrogen XPS (left) and NEXAFS (right) for bipyridine salts and co-crystals, showing the shift to high energy with proton transfer to nitrogen (salt formation) for both 1s binding energy (XPS) and 1s → 1π* energy (NEXAFS). Note that transition to higher order π* molecular orbitals in NEXAFS results in an additional low intensity resonance around 401 eV (clearly visible as a separate peak for the co-crystals and as asymmetry of the 1π* C═NH$^+$ peak for the salts).

Table 1. Nitrogen XPS and NEXAFS Peak Assignments and Positions[a]

			XPS N 1s binding energy, eV			NEXAFS N 1s→1π* energy, eV		
complex (base/acid)	ΔpK_a	d(N−H), Å	C═N	C═NH$^+$	shift	C═N	C═NH$^+$	shift
2BPY/BTA salt	2.48	0.916	399.15	401.54	+2.39	397.60	399.72	+2.12
4BPY/5-sulfosalicylic salt	3.87	0.962	399.40	401.33	+1.93	397.73	399.52	+1.79
4BPY/buTA co-crystal	−0.13	1.390	399.46			397.96		
4BPY/Phthalic co-crystal	0.32	1.449	399.41			397.85		
4BPY/Adipic co-crystal	−1.17	1.627	399.30			397.78		
4BPY/Thiodipropionic co-crystal	−0.76	1.673	399.26			397.75		
4BPY/Malonic co-crystal	0.44	1.798	399.20			397.71		

[a]Nitrogen−hydrogen distances are shown for C═NH$^+$ of the salts and C═N···HOOC of the co-crystals,[35−37] along with the ΔpK_a values [ΔpK_a = pK_a(base) − pK_a(acid)].[1,13,43,44]

and multiscan absorption corrections were carried out using the program CrysAlis RED (Oxford Diffraction Ltd., version 1.171.34.44, 2010). The structure was solved with SHELXS-97 and refined on F^2 against all reflections with SHELXL-97. All non-hydrogen atoms were refined by direct methods anisotropically; all hydrogen atoms were located in difference Fourier maps and refined isotropically. Full crystallographic details are provided within the CIF files in the Supporting Information, along with tables summarizing the main crystallographic data. The CIFs are also deposited with the Cambridge Crystallographic Data Centre (CCDC): CCDC 1038154 and 1038155 contain the supplementary crystallographic data for this paper. These data can be obtained free of charge from The Cambridge Crystallographic Data Centre via www.ccdc.cam.ac.uk/data_request/cif.

X-ray Photoelectron Spectroscopy (XPS). XP spectra of the powder samples (∼1 mg) were recorded with a Kratos Axis Ultra instrument employing a monochromatic Al Kα source (1486.69 eV).[21,38] High resolution spectra were measured within the spectral range of interest (ca. ±20 eV around the core level emission peaks) with 0.1 eV steps and 1000 ms dwell time per data point. Analysis of the data was carried out with Casa XPS software[39] using a Shirley background and GL(30) line shape (70% Gaussian, 30% Lorentzian).[39] Samples were referenced to the lowest E_B component C═C at 284.8 eV,[40] and the COOH/COO$^-$ peak position checked for successive scans; repeatability of the peak positions was within ±0.05 eV. Repeats were carried out to check for radiation damage.

Near Edge X-ray Absorption Fine Structure (NEXAFS) Spectroscopy. NEXAFS measurements were performed at the U7a beamline of the National Synchrotron Light Source (NSLS) at Brookhaven National Laboratory, NY. Partial electron yield (PEY) spectra for the nitrogen K-edge were collected via a channeltron electron multiplier with the sample (few mg) at the magic angle (54.7°) relative to the incident beam. An entrance grid bias of −150 V was used for PEY collection and a monochromator with a 600 lines/mm grating, providing energy resolution of ∼0.15 eV. After collection, the spectra were normalized by the simultaneously recorded drain current from an *in situ* gold-coated, 90% transmission grid (I_0) placed in the incident X-ray beam to eliminate the effect of incident beam intensity fluctuations and beamline optics absorption features. The monochromator energy scale was calibrated using the 400.6 eV first π* resonance of a titanium nitride grid located in the path of the incident X-ray beam. Repeatability of the peak positions was within ±0.05 eV. Repeats were carried out to check for radiation damage.

DOI: 10.1021/cg5018278
Cryst. Growth Des. 2015, 15, 1776−1783

RESULTS

XPS. XPS yields nitrogen 1s spectra with the binding energy (E_B) specific to the nitrogen chemical and local electronic environment and has recently been shown to be particularly adept at identifying the nature of intermolecular interactions (proton transfer vs H-bonding) in two-component base/acid systems.[14,18,19] Consequently, a single nitrogen 1s photoemission peak around 399.3 ± 0.1 eV is observed (Figure 2, left; Table 1) for the complexes of 4,4′-bipyridine with phthalic, adipic, thiodipropionic, and malonic acids (4BPY/phthalic, 4BPY/adipic, 4BPY/thio, 4BPY/malonic), reflecting the hydrogen bonded C═N nitrogen atoms of the bipyridine moiety in the co-crystals[36,37] (C═N···HOOC, Figure 3). XPS of 4,4′-bipyridine/1,2,3,4-butanetetracarboxylic acid (4BPY/buTA) also shows a single peak for the presence of C═N atoms and the formation of a co-crystal (Figures 2 and 3). For 2,2′-bipyridine/benzene-1,2,4,5-tetracarboxylic acid (2BPY/BTA), however, the photoemission signal is split into two peaks of approximately equal area, with a shift of around 2 eV to high energy for the new peak (Figure 2, left). With formation of a salt, nitrogen acquires a positive charge through proton transfer (donation of hydrogen) from the acid component: C═N → C═NH^+. The nitrogen XPS thus reveals that one of the nitrogen atoms of bipyridine has been protonated (C═NH^+), shifting its photoemission to higher energy (Table 1), in agreement with the single crystal X-ray diffraction (XRD) structure,[35] with 2BPY/BTA forming a NH^+, COO^- salt [$(2BPY^+)_2{\cdot}BTA^{2-}{\cdot}BTA$] (Figure 3). Comparison of the nitrogen XPS for the new complex of 4,4′-bipyridine/5-sulfosalicylic acid (4BPY/sulfo) shows two photoemission signals of equivalent area at 399.40 and 401.33 eV (Figure 2, left; Table 1), revealing that a proton has been transferred from 5-sulfosalicylic acid to one of the 4,4′-bipyridine nitrogen atoms, forming a 1:1 salt. This is confirmed by the subsequently obtained single crystal XRD, with 4BPY/sulfo involving NH^+, SO_3^- [BPY^+, $sulfo^-$] (Figure 3 and Supporting Information).

NEXAFS. Whereas XPS probes emission of an electron from the core N 1s level (Figure 4), the sharp resonances in the pre-edge region of NEXAFS arise from promotion of the N 1s electron to unoccupied valence orbitals of π^* character (N 1s → π^*, Figure 4). An edge (step up) in the spectrum occurs when sufficient energy is absorbed to promote the 1s electron beyond the ionization potential (IP) of its atom. Past the edge, some additional fine structure arises from broader σ^* shape resonances, which arise from multiple scattering of the electron off neighboring atoms. In the nitrogen K-edge spectra for the five co-crystals, the pyridine nitrogen C═N atoms result in the $1\pi^*$ resonance around 397.7 eV, arising from N 1s → LUMO (lowest unoccupied molecular orbital) transitions (N 1s → $1\pi^*$, Figure 2, right; Table 1), followed by a low intensity, higher order π^* resonance around 401 eV from transitions to higher-energy unoccupied π^* molecular orbitals. For the two salts, the $1\pi^*$ resonance around 397.7 eV arising from the C═N nitrogen environment is reduced in intensity and a second $1\pi^*$ resonance of half the intensity is visible at higher energy around 399.6 eV (Figure 2, right; Table 1). This shift to high energy reflects the change associated with proton transfer to nitrogen (C═NH^+, Figure 4), and the 1:1 ratio of the peaks (Figure 2, right) shows that only one of the two C═N nitrogen atoms of bipyridine has been protonated, in agreement with what was found by XPS and XRD (note that the higher order π^* resonance ∼401 eV also occurs for the salts, but is obscurred by the $1\pi^*$ C═NH^+ peak and thus presents as asymmetry toward high energy).

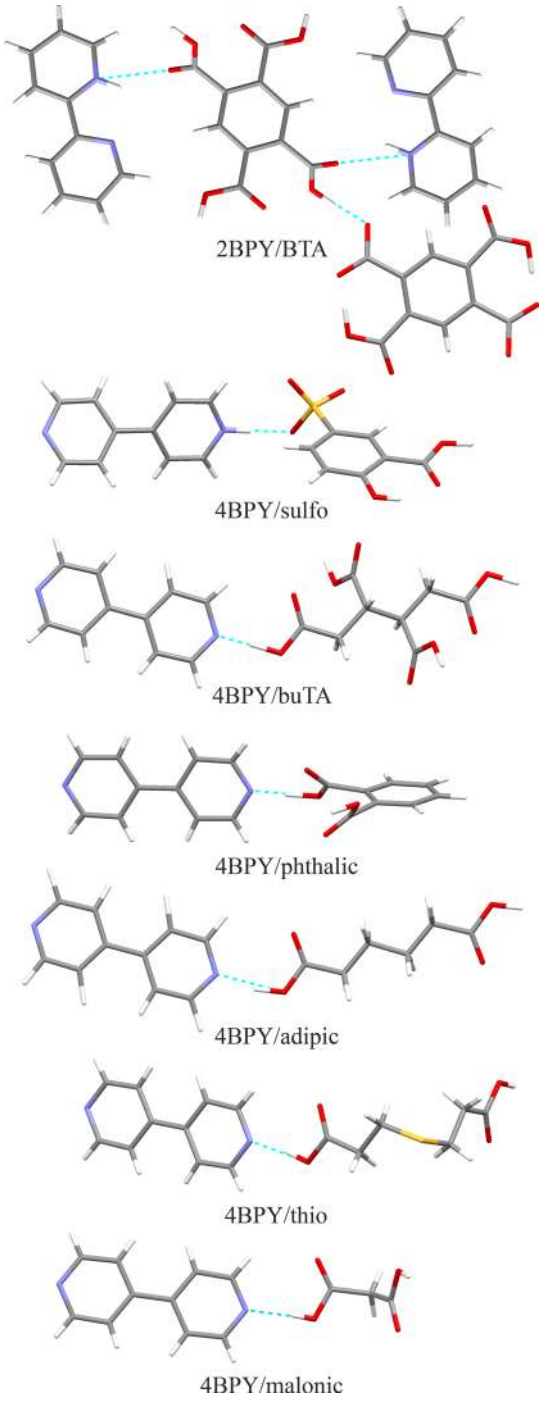

Figure 3. Aspects of the crystal structures of the salts and co-crystals, showing the stoichiometry and highlighting the nitrogen intermolecular hydrogen bonding between the base and acid molecules and protonation of nitrogen in the 2BPY/BTA and 4BPY/sulfo salts.

DISCUSSION

The ability to identify when protonation has occurred and distinguish between nitrogen-containing co-crystals and salts with nitrogen NEXAFS via π^* resonances is clearly demonstrated through comparisons with XPS and XRD (Figures 2 and 3), and for XPS and NEXAFS this can be prior to (or even in the absence of) crystal structure

DOI: 10.1021/cg5018278
Cryst. Growth Des. 2015, 15, 1776−1783

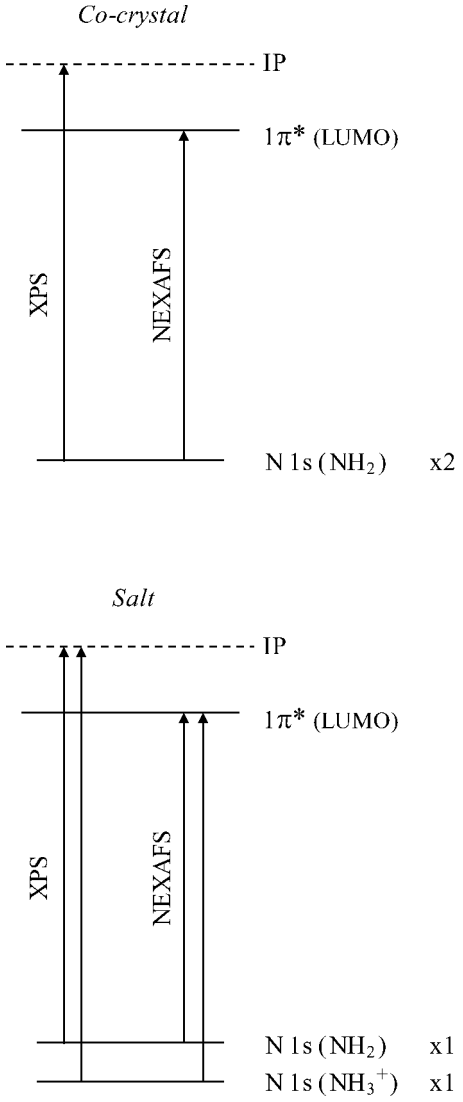

Figure 4. Schematic of photoemission from the nitrogen 1s core level for XPS such that the system is ionized through complete ejection of an electron and promotion from the nitrogen 1s core level to the lowest unoccupied molecular orbital (LUMO) for NEXAFS (N 1s → 1π*, where the antibonding π* MO is pulled below the ionization potential (IP) by the increased Coulomb potential on creation of a core hole[26]).

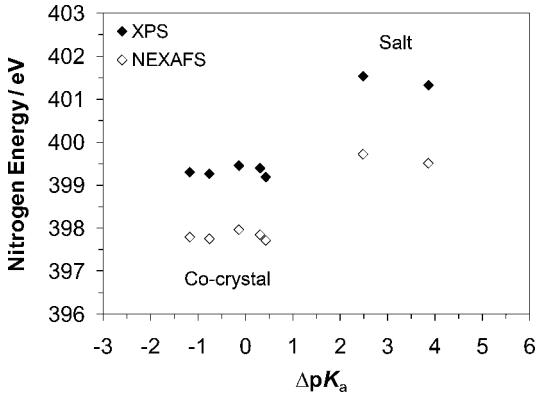

Figure 5. Correlation between the XPS N 1s binding energy and NEXAFS N 1s → 1π* energy and ΔpK_a, illustrating that both techniques clearly distinguish between protonated (salt) and unprotonated nitrogen (co-crystal). ΔpK_a = pK_a (base) − pK_a (acid).[1,13,43,44]

information. In recent years, pK_a differences have been used as a tool for predicting whether co-crystals or salts are expected [ΔpK_a = pK_a(base) − pK_a(acid)] and correlations with hydrogen bond strengths (including the proposed pK_a slide rule).[13,41,42] A plot of the XPS N 1s binding energies and NEXAFS N 1s → 1π* energies of the nitrogen acceptors of the seven base−acid systems as a function of ΔpK_a (Figure 5) shows the transition from hydrogen-bonding (associated with co-crystal formation) to proton transfer (salt formation) as the ΔpK_a increases through the region between 0 and +3, within which it is difficult to predict whether co-crystal or salt formation takes place.[13] For the current systems, the salts cover a range of ΔpK_a from 2.48 to 3.87 and the co-crystals −1.17 to 0.44 (with 4BPY/phthalic and 4BPY/malonic in the intermediate 0−3 region, Table 1). There is a clear separation between the respective XPS/NEXAFS nitrogen energies for the hydrogen bonded co-crystals and those for the protonated salts (Figure 5).[14,19] Both techniques unambiguously determine whether protonation has occurred, with a nitrogen energy difference of around +2 eV arising from protonation with both techniques (Figure 5).

In addition to identifying salt vs co-crystal, XPS and NEXAFS can provide information on cases associated with disorder. The previously reported XRD crystal structure of 4BPY/buTA[45] had short NHO hydrogen bonds (2.565(3) Å) and was refined as disordered over two distinct positions, with site occupancy of 0.59 (O−H···N with d(N−H) 1.73 Å) and 0.41 (O···H−N^+ with d(N−H) 0.88 Å). The XPS and NEXAFS in the current study show the presence of only one, sharp peak occurring in the region for C═N nitrogen atoms (Figure 2, Table 1). If there was any disorder of the NHO hydrogen bond, so that both C═N (O−H···N) and C═NH^+ (O···H−N^+) types of nitrogen environment were present, there would be a second, higher energy signal from C═NH^+ around 401.5 eV for XPS and 399.5 eV for NEXAFS (the ultrafast nature of the electronic transitions (~10^{-15}−10^{-16} s) means that every detected event represents a snapshot rather an average over vibrational, conformational, or structural changes, thereby permitting population analysis, even when transient species coexist[26,46−48]). Moreover, the relative (area) intensity of the two peaks would directly inform the site occupancy of hydrogen over the O−H···N and O···H−N^+ states. The complete absence of this peak here reveals no disorder in the product obtained from the current synthesis and redetermination, but rather a 1:1 co-crystal (confirmed by subsequent single crystal XRD, Figure 3 and Supporting Information) with a short nitrogen acceptor-hydrogen length of 1.39(4) Å for the NHO hydrogen bond (2.559(3) Å). The two structures were collected at the same temperature (100 K), negating the inference of temperature-related disorder. The differences in the products obtained in the previous[45] and current study are most likely attributable to the difficulty with which this complex is formed: recrystallization over several weeks is required to generate only a small amount of co-crystal product here while the previous crystallization generated disordered material[45] (and was not reproducible). It is also notable that the pK_a difference for 4BPY/buTA is extremely close to the range (ΔpK_a 0−3) for which salt/co-crystal is not easily predictable (−0.13, Table 1).

DOI: 10.1021/cg5018278
Cryst. Growth Des. 2015, 15, 1776−1783

Despite monitoring different electronic events (Figure 4), both XPS and NEXAFS illustrate their sensitivity to proton transfer and hydrogen bonding (Figure 2). The magnitude of the energy shifts observed to occur with Brønsted proton transfer to nitrogen (C═N → C═NH$^+$) with XPS and NEXAFS are very similar (Table 1), despite the different final state of the electron in both processes (free electron vs bound excited valence state) and thus the potentially differing influence of relaxation of energy levels following core excitation.[26] The shifts in the N 1s → 1π^* resonance energies in NEXAFS follow a similar trend to that of the photoemission 1s binding energies in XPS (Table 1), indicating that the initial-state nitrogen 1s core level shifts (chemical shifts, Figure 4) dominate over final-state effects, with only slightly smaller magnitudes in the NEXAFS shifts (Table 1).

Further comparison of the energy shifts between the signals arising from the two types of nitrogen in the salts (C═N and C═NH$^+$) reveals that the energy shift occurring with protonation is larger for 2BPY/BTA (+2.39 eV) than for 4BPY/sulfo (+1.93 eV) with XPS, and this is also reflected in the NEXAFS shifts (Table 1), visible as a widening separation between the peaks arising from C═N and C═NH$^+$ nitrogen environments (Figure 2). In the 2BPY/BTA salt, single crystal XRD[35] shows the donated hydrogen (from COOH) to be closer to nitrogen than that donated by SO_3H in the 4BPY/sulfo salt (Table 1). This can be viewed as a more complete proton transfer from the acid and leads to decreased electron density (higher effective positive charge) at the protonated nitrogen C═NH$^+$ for 2BPY as it interacts more strongly with the hydrogen atom. More energy must therefore be provided to eject or promote a nitrogen core electron, leading to the higher C═NH$^+$ energy for 2BPY/BTA compared with 4BPY/sulfo (Figure 6). Interestingly, the energy for the remaining, non-protonated C═N bipyridine nitrogen in the salts is slightly reduced for 2BPY/BTA compared with 4BPY/sulfo in both techniques (perhaps slightly more evident with XPS, Table 1), and this may be related to the nature of the hydrogen bonding (or differing electron density around nitrogen with varying position within the pyridine rings). In the 2,2′-bipyridine system, the non-protonated C═N nitrogen is involved in a long, intramolecular bridging C═N···H−N$^+$ (between the two 2,2′-nitrogen atoms, d(N−H) 2.189 Å),[35] as opposed to the shorter intermolecular C═N···H−O in 4BPY/sulfo (d(N−H) 1.461 Å, Supporting Information), and variation in hydrogen bonding interactions can lead to small decreases in energy of this magnitude.[14,24,25,49]

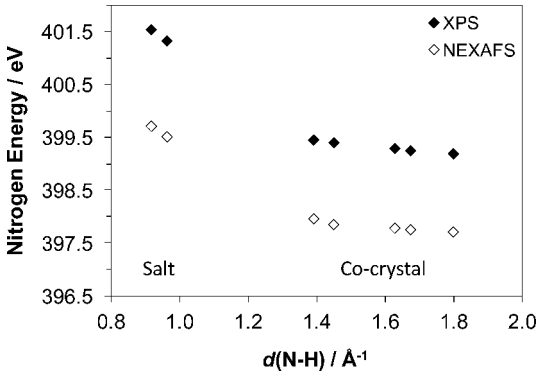

Figure 6. Relationship between the N 1s core level binding energies (XPS) and N 1s → 1π^* transitions (NEXAFS) with the distance between the Brønsted donor hydrogen of the acid and acceptor nitrogen of the bipyridine base.

Closer inspection of the N 1s binding energies and N 1s → 1π^* energies for the C═N nitrogen of the co-crystals shows a small yet successively higher energy occurs with a shorter distance between the H-bonded acceptor nitrogen of 4,4′-bipyridine and hydrogen of the acid molecule (N···H−O, Figure 6, Table 1). Indeed, there is a term in the potential model for XPS relating to atomic distances in addition to charge,[50] and there are initial computational results indicative of a dependence of core level energy on hydrogen bond distances for oxygen.[24] Considering the nitrogen−hydrogen distance to be a measure of the extent to which nitrogen interacts with the hydrogen (or the extent of proton transfer from the acid COOH), this effect appears enough to be reflected in the chemical shifts (Figure 6).

The identification of whether a salt or co-crystal has been formed can be particularly important in terms of regulatory requirements in the pharmaceutical industry,[4,17] and the nature and nitrogen state stoichiometry of the complex provided by NEXAFS adds it to one of only a few techniques capable of unambiguous assignment.[20] The level of sensitivity shown for the nitrogen XPS and NEXAFS chemical shifts, through their dependence on the nitrogen−hydrogen bond length and a clear method of detecting the presence of disordered NHO hydrogen bonds, widens the use of these techniques to more crystallographic applications.

CONCLUSIONS

The ability of nitrogen NEXAFS to identify Brønsted proton transfer and therefore co-crystals vs salts has been illustrated for bipyridine systems alongside XPS. Additional π^* (NEXAFS) and N 1s photoemission (XPS) peaks occur when proton transfer from the acid to nitrogen of the base results in the formation of a salt (C═NH$^+$). The intensity ratio between the peaks associated with the protonated and unprotonated form (C═N) provides the stoichiometry between the two. The absence of the C═NH$^+$ peak for the 4,4′-bipyridine/1,2,3,4-butanetetracarboxylic acid system reveals that no disorder across the NHO hydrogen bond is present in the sample synthesized for this study, in contrast to previously obtained disordered material, while the product of crystallization of 4,4-bipyridine with 5-sulfosalicylic acid was identified as a 1:1 salt. The similarity of the chemical shifts for NEXAFS with XPS indicates that the core level (initial-state) tends to dominate in these organic systems. Comparison of the XPS and NEXAFS nitrogen resonances with ΔpK_a values clearly shows the transition from co-crystal to salt, with a shift of around +2 eV for protonation of nitrogen. There is also a monotonic dependence of the chemical shifts on the nitrogen−hydrogen distance (or amount of proton transfer) and the nature of hydrogen bonding at the non-protonated nitrogen. This demonstrates the sensitivity of NEXAFS to proton transfer (Brønsted donation) and provides insight into the local interactions of hydrogen with nitrogen, and more widely, the important influence of the chemical state on the π^* region of NEXAFS.

ASSOCIATED CONTENT

Supporting Information

X-ray crystallographic information files (CIF) for the new 4′4-bipyridine/5-sulfosalicylic acid (4BPY/sulfo) salt and 4,4′bipyridine/1,2,3,4-butanetetracarboxylic acid (4BPY/buTA) co-

DOI: 10.1021/cg5018278
Cryst. Growth Des. 2015, 15, 1776−1783

crystal, along with tables summarizing the crystallographic data and powder XRD patterns for the co-crystals and salts. This material is available free of charge via the Internet at http://pubs.acs.org. Crystallographic information files are also available from the Cambridge Crystallographic Data Centre (CCDC) upon request (http://www.ccdc.cam.ac.uk, CCDC deposition numbers 1038154−1038155).

AUTHOR INFORMATION

Corresponding Authors

*Joanna S. Stevens. Tel: +44 (0)161-306-4362. E-mail: joanna.stevens@manchester.ac.uk.

*Sven L. M. Schroeder. Tel: +44 (0)113-343-2401. Fax +44 (0)113-343-2384. E-mail: s.l.m.schroeder@leeds.ac.uk.

Notes

The authors declare no competing financial interest.

ACKNOWLEDGMENTS

We acknowledge funding from the EPSRC under the previous PhD+ fellowship for J.S.S. and current support for J.S.S. and S.L.M.S. through the Critical Mass Grant EP/1013563/1. NEXAFS beamtime was provided at the U7a beamline of the National Synchrotron Light Source (NSLS), NY. Use of the National Synchrotron Light Source, Brookhaven National Laboratory, was supported by the U.S. Department of Energy, Office of Science, Office of Basic Energy Sciences, under Contract No. DE-AC02-98CH10886. L.K.N. acknowledges financial support from EPSRC through a DTA Ph.D. studentship and the NowNano Doctoral Training Centre (Grant Number EP/G03737X/1).

REFERENCES

(1) *Handbook of Pharmaceutical Salts: Properties, Selection, and Use*; Wiley-VCH: Weinheim, Germany, 2002.

(2) Schultheiss, N.; Newman, A. *Cryst. Growth Des.* **2009**, *95*, 499−516.

(3) Vishweshwar, P.; McMahon, J. A.; Bis, J. A.; Zaworotko, M. J. *J. Pharm. Sci.* **2006**, *95*, 499−516.

(4) *Pharmaceutical Salts and Co-crystals*; The Royal Society of Chemistry: Cambridge, U.K., 2012.

(5) Horiuchi, S.; Kumai, R.; Tokura, Y. *Chem. Commun.* **2007**, 2321−2329.

(6) Bolton, O.; Matzger, A. J. *Angew. Chem., Int. Ed.* **2011**, *50*, 8960−8963.

(7) Jones, C. L.; Wilson, C. C.; Thomas, L. H. *CrystEngComm* **2014**, *16*, 5849−5858.

(8) Yan, D.; Bučar, D.-K.; Delori, A.; Patel, B.; Lloyd, G. O.; Jones, W.; Duan, X. *Chem.—Eur. J.* **2013**, *19*, 8213−8219.

(9) Yan, D.; Fan, G.; Guan, Y.; Meng, Q.; Li, C.; Wang, J. *Phys. Chem. Chem. Phys.* **2013**, *15*, 19845−19852.

(10) Gilli, G.; Gilli, P. *The Nature of the Hydrogen Bond*; Oxford University Press: Oxford, U.K., 2009.

(11) Wilson, C. *Crystallogr. Rev.* **2007**, *13*, 143−198.

(12) Aakeröy, C. B.; Fasulo, M. E.; Desper, J. *Mol. Pharmaceutics* **2007**, *4*, 317−322.

(13) Childs, S. L.; Stahly, G. P.; Park, A. *Mol. Pharmaceutics* **2007**, *4*, 323−338.

(14) Stevens, J. S.; Byard, S. J.; Seaton, C. C.; Sadiq, G.; Davey, R. J.; Schroeder, S. L. M. *Phys. Chem. Chem. Phys.* **2014**, *16*, 1150−1160.

(15) Taylor, R.; Kennard, O. *Acta Crystallogr., Sect. B: Struct. Sci.* **1983**, *39*, 133−138.

(16) Schmidtmann, M.; Coster, P.; Henry, P. F.; Ting, V. P.; Weller, M. T.; Wilson, C. C. *CrystEngComm* **2014**, *16*, 1232−1236.

(17) FDA Guidance for Industry: Regulatory Classification of Pharmaceutical Co-crystals; Food and Drug Administration: Silver Spring, MD, http://www.fda.gov/downloads/Drugs/Guidances/UCM281764.pdf, 2013.

(18) Stevens, J. S.; Byard, S. J.; Schroeder, S. L. M. *J. Pharm. Sci.* **2010**, *99*, 4453−4457.

(19) Stevens, J. S.; Byard, S. J.; Seaton, C. C.; Sadiq, G.; Davey, R. J.; Schroeder, S. L. M. *Angew. Chem., Int. Ed.* **2011**, *50*, 9916−9918.

(20) Stevens, J. S.; Byard, S. J.; Muryn, C. A.; Schroeder, S. L. M. *J. Phys. Chem. B* **2010**, *114*, 13961−13969.

(21) Stevens, J. S.; Byard, S. J.; Schroeder, S. L. M. *Cryst. Growth Des.* **2010**, *10*, 1435−1442.

(22) Stevens, J. S.; de Luca, A. C.; Pelendritis, M.; Terenghi, G.; Downes, S.; Schroeder, S. L. M. *Surf. Interface Anal.* **2013**, *45*, 1238−1246.

(23) Bagus, P. S.; Illas, F.; Casanovas, J. *Chem. Phys. Lett.* **1997**, *272*, 168−172.

(24) Tu, G.; Tu, Y.; Vahtras, O.; Agren, H. *Chem. Phys. Lett.* **2009**, *468*, 294−298.

(25) Garcia-Gil, S.; Arnau, A.; Garcia-Lekue, A. *Surf. Sci.* **2013**, *613*, 102−107.

(26) Stöhr, J. *NEXAFS Spectroscopy*; Springer-Verlag: Berlin, 1992.

(27) Lehmann, J.; Solomon, D.; Brandes, J.; Fleckenstein, H.; Jacobson, C.; Thieme, J., Synchrotron-Based Near-Edge X-Ray Spectroscopy of Natural Organic Matter in Soils and Sediments. In *Biophysico-Chemical Processes Involving Natural Nonliving Organic Matter in Environmental Systems*; Senesi, N., Xing, B., Huang, P. M., Eds.; John Wiley & Sons, Inc.: Hoboken, NJ, 2009; Chapter 17, pp 741−748.

(28) Solomon, D.; Lehmann, J.; Kinyangi, J.; Liang, B.; Heymann, K.; Dathe, L.; Hanley, K.; Wirick, S.; Jacobsen, C. *Soil Sci. Soc. Am. J.* **2009**, *73*, 1817−1830.

(29) Leinweber, P.; Kruse, J.; Walley, F. L.; Gillespie, A.; Eckhardt, K.-U.; Blyth, R. I. R.; Regier, T. *J. Synchrotron Radiat.* **2007**, *14*, 500−511.

(30) Vairavamurthy, A.; Wang, S. *Environ. Sci. Technol.* **2002**, *36*, 3050−3056.

(31) Cooney, R. R.; Urquhart, S. G. *J. Phys. Chem. B* **2004**, *108*, 18185−18191.

(32) Urquhart, S. G.; Ade, H. *J. Phys. Chem. B* **2002**, *106*, 8531−8538.

(33) Stevens, J. S.; Seabourne, C. R.; Jaye, C.; Fischer, D. A.; Scott, A. J.; Schroeder, S. L. M. *J. Phys. Chem. B* **2014**, *118*, 12121−12128.

(34) Booth, A. M.; Braun, S.; Lonsborough, T.; Purton, J.; Patel, S.; Schroeder, S. L. M. *AIP Conf. Proc.* **2007**, *882*, 325−327.

(35) Mrvos-Sermek, D.; Popovic, Z.; Matkovic-Calogovic, D. *Acta Crystallogr., Sect. C: Cryst. Struct. Commun.* **1996**, *52*, 2538−2541.

(36) Tomura, M.; Yamashita, Y. *Chem. Lett.* **2001**, *30*, 532−533.

(37) Pedireddi, V. R.; Chatterjee, S.; Ranganathan, A.; Rao, C. N. R. *Tetrahedron* **1998**, *54*, 9457−9474.

(38) Stevens, J. S.; Schroeder, S. L. M. *Surf. Interface Anal.* **2009**, *41*, 453−462.

(39) Fairley, N.; Carrick, A. *The Casa Cookbook - Part 1: Recipes for XPS Data Processing*; Acolyte Science: Knutsford, Cheshire, 2005.

(40) *The XPS of Polymers Database*; Surface Spectra Ltd.: Manchester, 2000.

(41) Gilli, P.; Pretto, L.; Gilli, G. *J. Mol. Struct.* **2007**, *844−845*, 328−339.

(42) Gilli, P.; Pretto, L.; Bertolasi, V.; Gilli, G. *Acc. Chem. Res.* **2009**, *42*, 33−44.

(43) Experimental pK_a values were obtained using the ACD/I-Lab Web service: *ACD/pKa DB 12.0*; Advanced Chemistry Development, Inc. (ACD/Labs): Toronto, 2010.

(44) Predicted pK_a values were obtained using: *ACD/PhysChem. Suite v12.0*; Advanced Chemistry Development, Inc. (ACD/Labs): Toronto, 2010.

(45) Najafpour, M. M.; Holynska, M.; Lis, T. *Acta Crystallogr., Sect. E: Struct. Rep. Online* **2008**, *64*, o985.

(46) Sawatzky, G. A.; Antonides, E. *J. Phys., Colloq.* **1976**, *37*, C4-117−C4-123.

DOI: 10.1021/cg5018278
Cryst. Growth Des. 2015, 15, 1776−1783

(47) Nolting, D.; Ottosson, N.; Faubel, M.; Hertel, I. V.; Winter, B. *J. Am. Chem. Soc.* **2008**, *130*, 8150−8151.
(48) Ito, E.; Oji, H.; Araki, T.; Oichi, K.; Ishii, H.; Ouchi, Y.; Ohta, T.; Kosugi, N.; Maruyama, Y.; Naito, T.; Inabe, T.; Seki, K. *J. Am. Chem. Soc.* **1997**, *119*, 6336−6344.
(49) Bisti, F.; Stroppa, A.; Picozzi, S.; Donarelli, M.; Picozzi, S.; Coreno, M. *J. Chem. Phys.* **2013**, *138*, No. 014308.
(50) Siegbahn, K.; Nordling, C.; Fahlman, A.; Nordberg, R.; Hamrin, K.; Hedman, J.; Johansson, G.; Bergmark, T.; Karlsson, S.-E.; Lindgren, I.; Lindberg, B. *ESCA: Atomic, Molecular and Solid State Structure Studied by Means of Electron Spectroscopy*; Almqvist & Wiksells Boktryckeri AB: Uppsala, Sweden, 1967; Vol. *20*.

DOI: 10.1021/cg5018278
Cryst. Growth Des. 2015, 15, 1776−1783